RadioGraphics

US of the Major Salivary Glands: Anatomy and Spatial Relationships, Pathologic Conditions, and Pitfalls[1]

Ewa J. Bialek, MD, PhD • Wieslaw Jakubowski, MD, PhD • Piotr Zajkowski, MD, PhD • Kazimierz T. Szopinski, MD, PhD • Antoni Osmolski, MD, PhD

TEACHING POINTS
See last page

Ultrasonography (US) is useful for differential diagnosis of diseases of the salivary glands. In acute inflammation, salivary glands are enlarged and hypoechoic with increased blood flow; they may contain multiple small, oval, hypoechoic areas. In chronic inflammation, salivary glands are normal sized or smaller, hypoechoic, and inhomogeneous. Sialolithiasis appears as markedly hyperechoic lines or points with distal acoustic shadowing. Sialosis appears as enlarged hyperechoic glands without focal lesions or increased blood flow. The US features of advanced Sjögren syndrome include inhomogeneous salivary glands with scattered small, oval, hypoechoic or anechoic areas, usually well defined, and increased parenchymal blood flow. Pleomorphic adenomas are usually hypoechoic, well-defined, lobulated lesions with posterior acoustic enhancement that may contain calcifications; Warthin tumors are usually oval, hypoechoic, well-defined lesions that often contain anechoic areas and are often hypervascularized. Malignant neoplasms of the salivary glands may have irregular shapes, irregular borders, blurred margins, and a hypoechoic inhomogeneous structure or may have a benign appearance. Salivary gland cysts have well-defined margins, anechoic contents, posterior acoustic enhancement, and no internal blood flow. However, US appearances of some diseases may overlap, thus producing diagnostic pitfalls.

Abbreviation: HIV = human immunodeficiency virus

RadioGraphics 2006; 26:745–763 • **Published online** 10.1148/rg.263055024 • **Content Codes:** HN NR US

[1]From the Department of Diagnostic Imaging, Second Faculty of Medicine, Medical University of Warsaw, ul. Kondratowicza 8, 03-242 Warsaw, Poland (E.J.B., W.J., P.Z., K.T.S.); and the Department of Otolaryngology, Center of Postgraduate Medical Education, Warsaw, Poland (A.O.). Recipient of an Excellence in Design award for an education exhibit at the 2004 RSNA Annual Meeting. Received February 8, 2005; revision requested March 18 and received November 8; accepted November 9. All authors have no financial relationships to disclose. **Address correspondence to** E.J.B. (e-mail: *ewajbmd@go2.pl*).

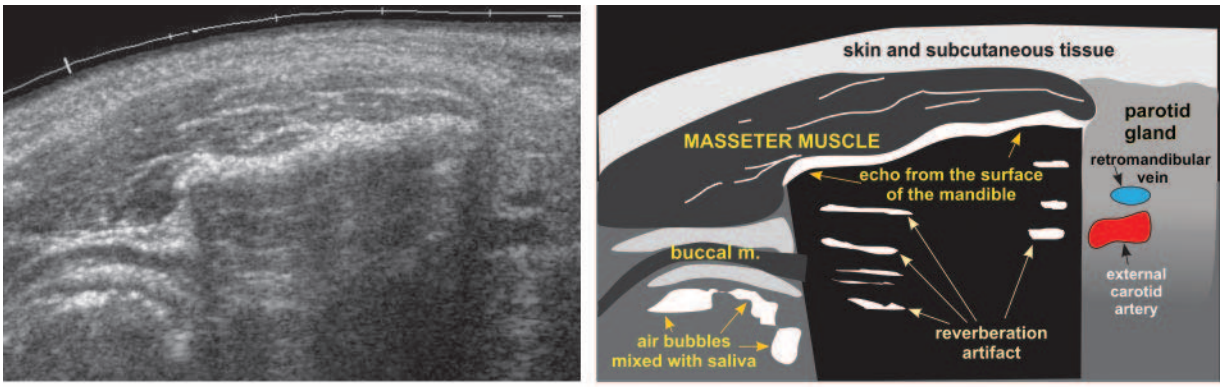

Figure 1. Transverse panoramic US image **(a)** and corresponding diagram **(b)** show the normal anatomy of the left parotid gland and part of the cheek. *m* = muscle.

Introduction

The algorithm proposed in the United States for imaging of salivary glands includes nonenhanced and contrast-enhanced computed tomography (CT), nonenhanced and contrast-enhanced magnetic resonance (MR) imaging, and sialography (also MR sialography), applied in a different order depending on clinical data (1,2). In general, CT is considered the best single method for assessment of inflammatory diseases and MR imaging is considered the best single method for assessment of salivary gland tumors (1–3). According to Yousem et al (2) ultrasonography (US) is underused in most North American sites, but in experienced hands it may supplant both CT and MR in imaging of superficial salivary gland lesions.

In Europe and Asia, US is widely accepted as the first imaging method for assessment of lymph nodes and soft-tissue diseases in the head and neck, including major salivary glands (4–7). Results of the US examination alone may suggest the final diagnosis or supply important differential diagnostic data. As the head and neck region has a complex anatomic structure, a sound knowledge of sonographic anatomy and spatial relationships is crucial for reliable performance of the examination. Also, knowledge of the sonographic features of the most common diseases in this area is a requisite.

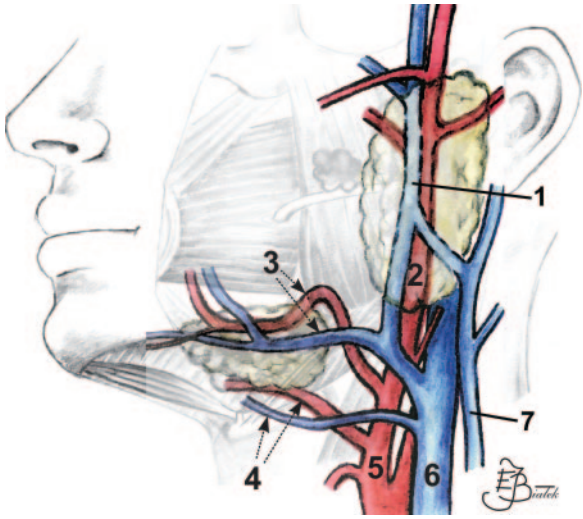

Figure 2. Drawing shows the major blood vessels in the area of the salivary glands. *1* = retromandibular vein, *2* = external carotid artery, *3* = facial artery and vein, *4* = lingual artery and vein, *5* = external carotid artery, *6* = internal jugular vein, *7* = external jugular vein.

It is sometimes not possible to visualize examined lesions completely at US because of their location, penetrating to the deep lobe of the parotid gland or behind the acoustic shadow of the mandible. In these situations, performance of further imaging examinations—CT or MR imag-

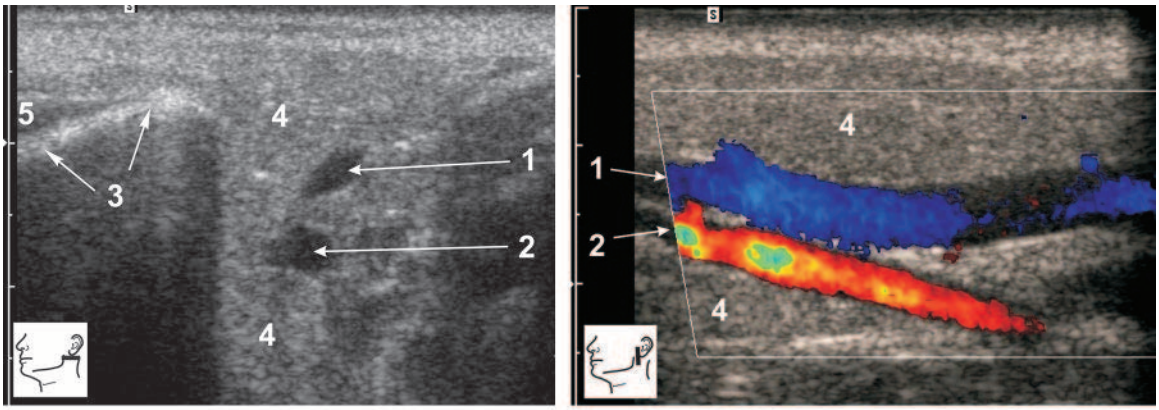

a. b.

Figure 3. Transverse **(a)** and longitudinal **(b)** US images show the normal anatomy of the left parotid gland. The positions of the US probe are shown in the inset diagrams. *1* = retromandibular vein, *2* = external carotid artery, *3* = echo from the surface of the mandible, *4* = parotid gland, *5* = masseter muscle.

ing—is warranted. Also, in cases of suspected malignant lesions, further diagnostic methods (ie, CT or MR imaging) should be applied to assess possible infiltration of bones or deep structures invisible at US (the base of the skull, parapharyngeal space) and to evaluate deep-lying lymph nodes (1,3,8,9). On the other hand, dynamic scintigraphy is still the method of choice in functional evaluation of the salivary glands (10,11).

In this article, we present the anatomy of the major salivary glands and neighboring structures as seen at US, as well as the US features of the most common pathologic conditions affecting the parotid and submandibular glands. These conditions include inflammatory diseases, sialolithiasis, sialosis, Sjögren syndrome, neoplasms, cysts, and trauma, as well as the effects of irradiation.

Technique

The examination should be carried out with the highest-frequency transducer possible. Usually, 5–12-MHz wide-band linear transducers (median frequency, 7–7.5 MHz or more) are used (9). In assessment of large tumors and lesions located in deep portions of the glands, 5–10-MHz transducers may be useful (12). Probes with a median frequency above 10 MHz may be useful in evaluation of the internal structure of salivary glands (12,13).

Entire salivary glands and all lesions have to be evaluated in at least two perpendicular planes during a US examination. The whole neck should also be scanned to assess lymph nodes and search for concomitant or related disease.

Anatomy

Parotid Gland

The parotid gland is located in the retromandibular fossa, anterior to the ear and sternocleidomastoid muscle. Parts of the superficial lobe cover the ramus of the mandible and the posterior part of the masseter muscle (Fig 1).

The border between the superficial and deep parotid lobes is created by a plane in which the facial nerve and its branches are located. Branches of the facial nerve are not visible at US. Parts of the trunk of this nerve may be demonstrated only with high-frequency probes (above 10 MHz) (13). Therefore, the retromandibular vein, which usually lies directly above the trunk of the facial nerve (14), is used as a US landmark separating the superficial and deep lobes of the parotid gland (Figs 2–4). Although the extracranial portion of the facial nerve may be visualized on high-resolution MR images (15), the retromandibular vein is commonly used as an anatomic landmark in preoperative CT and MR imaging examinations of parotid neoplasms (16). The deep parotid lobe can be visualized only partially at US. Some areas of glandular parenchyma and possible lesions may be hidden in the acoustic shadow behind the mandibular ramus (Fig 4).

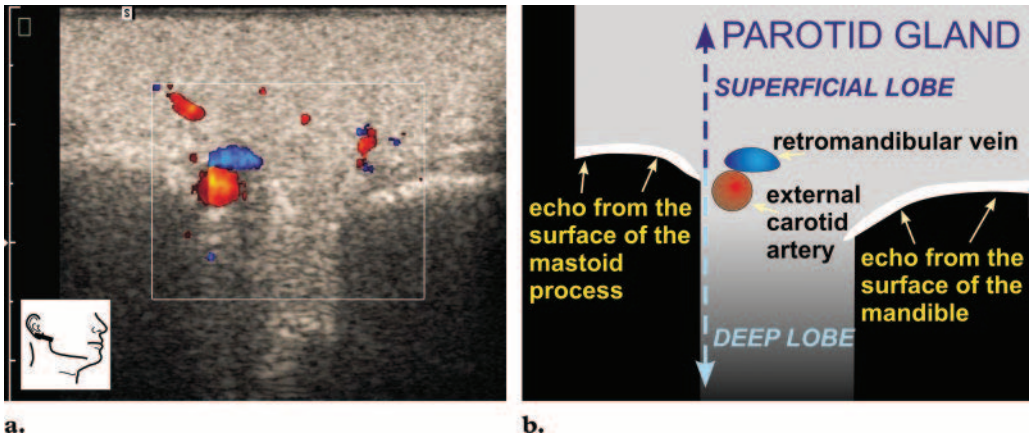

Figure 4. Transverse US image of the right parotid gland **(a)** and corresponding diagram **(b)** show the border between the superficial and deep lobes of the gland. The position of the US probe is shown in the inset diagram.

The normal echogenicity of all major salivary glands, including the parotid gland, is generally homogeneous and varies from very bright and markedly hyperechoic to only slightly hyperechoic in comparison to adjacent muscles. The echogenicity of the parotid gland depends on the amount of intraglandular fatty tissue. Salivary glands with high fat content are hyperechoic in comparison to surrounding muscles and markedly suppress ultrasound waves, so that the deep lobe is inaccessible for US assessment and sometimes even large vessels crossing the parotid gland—the retromandibular vein and external carotid artery—are barely visible or not visible at all on gray-scale images (Fig 5).

After leaving the parotid gland, the main excretory duct (Stenon duct) lies on the masseter muscle, about 1 cm below the zygomatic arch, then crosses the buccal muscle and has its orifice in the parotid papilla at the level of the upper second molar. The length of the Stenon duct usually varies between 3 and 5 cm. A nondilated duct is usually not visible during US examination (Fig 6). However, some authors report showing intraglandular nondilated parts of the Stenon duct with high-resolution US (13).

Along the course of the Stenon duct in the soft tissues of the cheek, an accessory parotid gland may be found, unilaterally or bilaterally. The accessory parotid gland may also be the site of salivary gland tumors, benign or malignant (17,18).

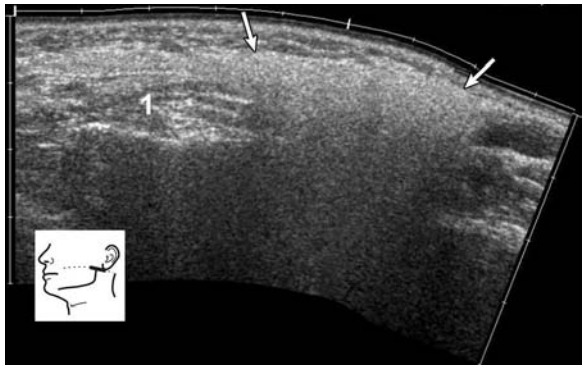

Figure 5. Transverse panoramic US image of the left parotid gland (arrows) and cheek shows that the gland has a high fat content. The parenchyma is hyperechoic with marked suppression of ultrasound waves, and no vessels are visible. The position of the US probe is shown in the inset diagram. *1* = masseter muscle.

In the parenchyma of the parotid gland, lymph nodes may be found (19). They are localized mainly in the area of the upper and lower poles of the gland. Normal intraparotid lymph nodes may be oval or have a longitudinal shape (Fig 7). Almost 60% of parotid nodes have a short axis–to–long axis ratio greater than 0.5. The presence of a hyperechoic hilum is one of the important criteria for the normality of parotid lymph nodes (Fig 7).

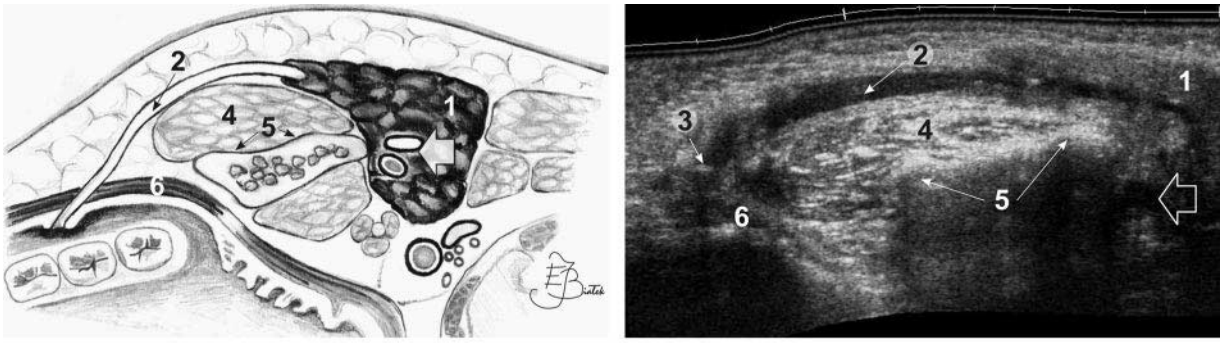

a. b.

Figure 6. **(a)** Diagram shows the location of the Stenon duct. *1* = parotid gland, *2* = Stenon duct, *4* = masseter muscle, *5* = surface of the mandible, *6* = buccal muscle, large arrow = retromandibular vein and external carotid artery. **(b)** Panoramic US image shows a dilated Stenon duct in a patient with sialolithiasis and inflammation. *1* = inflamed left parotid gland, *2* = dilated Stenon duct, *3* = stone, *4* = masseter muscle, *5* = surface of the mandible, *6* = buccal muscle, large arrow = retromandibular vein and external carotid artery.

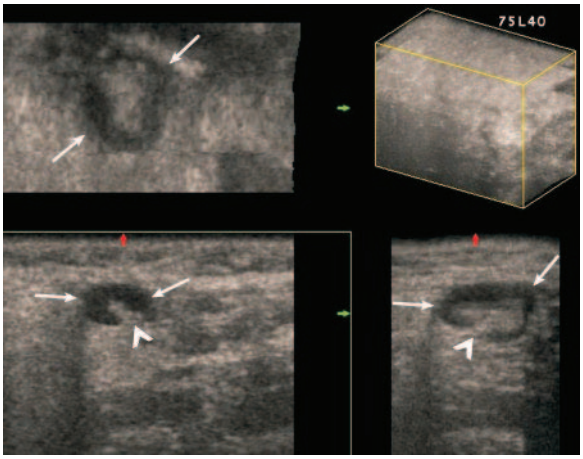

Figure 7. Three-dimensional US images show a normal intraparotid lymph node (arrows), which is oval with a homogeneous cortex and a central hyperechoic hilum. The hilum is connected to surrounding connective tissue (arrowhead).

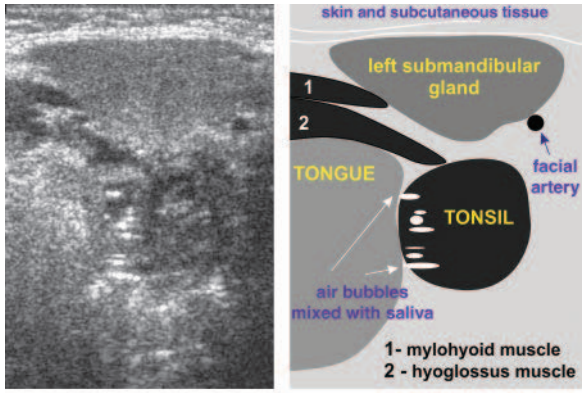

a. b.

Figure 8. US image obtained obliquely relative to the mandible **(a)** and corresponding diagram **(b)** show the left submandibular gland with surrounding structures.

Their short axis should not exceed 5–6 mm in the normal state (6,7). With the application of sensitive power Doppler US, central vessels may be seen in normal parotid lymph nodes.

Submandibular Gland

The submandibular gland lies in the posterior part of the submandibular triangle. The sides of the submandibular triangle are created by the anterior and posterior bellies of the digastric muscle and the body of the mandible. The space anterior to the submandibular gland is occupied by connective tissue and lymph nodes. Generally, the shape of the submandibular gland in longitudinal and transverse sections is close to a triangle (Fig 8). The submandibular gland may be connected with the parotid or sublingual gland by the glandular processes.

The facial artery may cross the parenchyma of the submandibular gland in its tortuous course (Fig 9). The facial vein runs along the anterosuperior part of the submandibular gland. In its

Figure 9. US image shows the tortuous facial artery (arrowheads) crossing the parenchyma of the right submandibular gland (arrows).

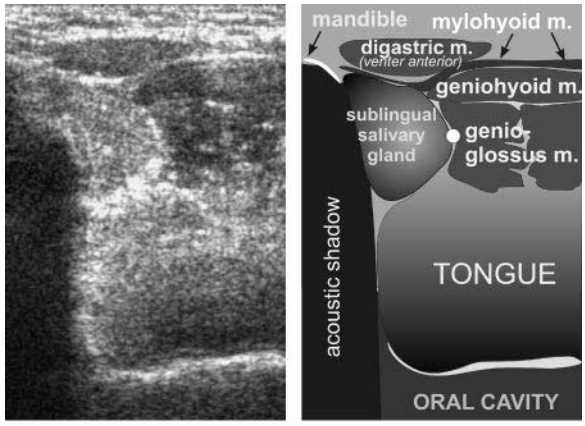

a. b.

Figure 11. Transverse US image **(a)** and corresponding diagram **(b)** show the sublingual gland and its surrounding structures. White circle = Wharton duct, *m* = muscle.

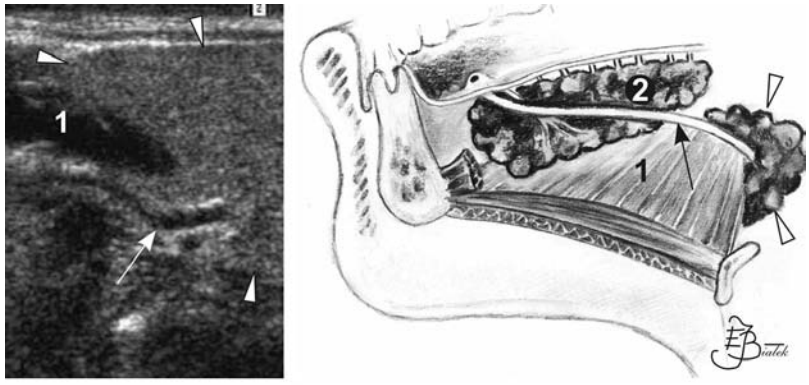

a. b.

Figure 10. **(a)** US image shows a nondilated Wharton duct (arrow) in a slim patient. Arrowheads = submandibular gland, *1* = mylohyoid muscle. **(b)** Diagram shows the course of the Wharton duct (arrow). Arrowheads = submandibular gland, *1* = mylohyoid muscle, *2* = sublingual gland.

posterior portion, a branch connecting with the retromandibular vein may be found (Fig 2). Medially to the submandibular gland run the lingual artery and vein.

The submandibular excretory duct (Wharton duct) runs from the area of the submandibular gland hilum at the level of the border of the mylohyoid muscle, then bends around the free part of the mylohyoid muscle and extends to its orifice at the sublingual caruncle along the medial part of the sublingual gland. In general, a nondilated duct is not visible at US, but sometimes in slim individuals it may be visible (Fig 10).

In some patients (obese patients, those who have undergone neck irradiation), the submandibular parenchyma may suppress ultrasound waves to such an extent that it is not possible to show not only deeper-lying structures but also the lower outline of the submandibular gland.

Sublingual Gland

The sublingual gland lies between the muscles of the oral cavity floor: the geniohyoid muscle, intrinsic muscles of the tongue, and hyoglossal muscle (medially) and the mylohyoid muscle. Its lateral side is adjacent to the mandible. On transverse sections, the shape of the sublingual gland is close to an oval (Fig 11); on sections parallel to the body of the mandible, the shape is longitudinal and lentiform. Along its medial part runs the excretory duct of the submandibular gland.

Inflammatory Diseases

Inflammatory diseases are the most common diseases affecting the major salivary glands (1,3).

Acute Inflammation

Acute inflammation causes painful swelling of the salivary gland, often bilaterally. Viral salivary gland infections are the most common in children. A particular predilection for the salivary

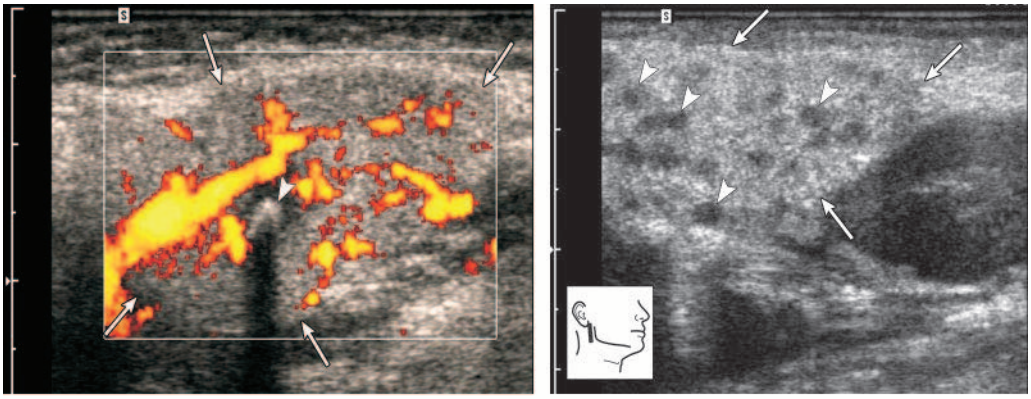

12. 13.

Figures 12, 13. **(12)** Power Doppler US image shows an acutely inflamed right submandibular gland (arrows) containing a stone (arrowhead). The gland is enlarged and hypoechoic with rounded edges and increased blood flow. **(13)** Gray-scale US image shows an acutely inflamed right parotid gland (arrows) in a 5-year-old child. The gland is enlarged and inhomogeneous with multiple small, oval, hypoechoic areas (arrowheads). The position of the US probe is shown in the inset diagram.

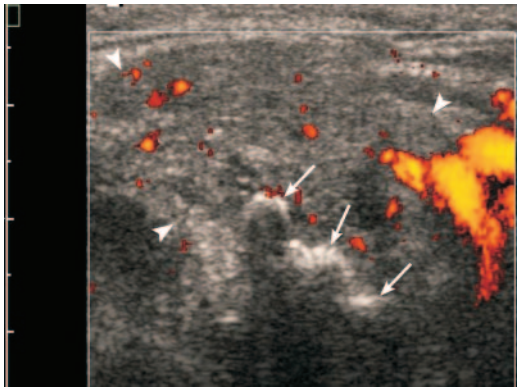

Figure 14. Power Doppler US image shows chronic inflammation of the left submandibular gland (arrowheads). The gland is inhomogeneous with decreased parenchymal echogenicity but without increased blood flow. Arrows = stones.

glands is shown by mumps virus and cytomegalovirus (20). Acute bacterial infections are usually caused by *Staphylococcus aureus* or oral flora (21).

Teaching Point

In acute inflammation, salivary glands are enlarged and hypoechoic. They may be inhomogeneous; may contain multiple small, oval, hypoechoic areas; and may have increased blood flow at US (Figs 12, 13) (9,22–25). Enlarged lymph nodes with increased central blood flow may be observed in acute inflammation of salivary glands (26).

Abscess

During acute sialadenitis, abscess formation may take place. Predisposing factors include dehydration and excretory duct obstruction caused by stones or fibrosis (27). At clinical examination, abscesses may be difficult to detect. They usually manifest as painful swelling of the salivary gland with skin reddening (28). The typical fluctuation sign may be absent in about 70% of cases (28).

At US, abscesses are hypoechoic or anechoic lesions with posterior acoustic enhancement and unclear borders (22,28). Central liquefaction may be distinguished as an avascular area or identified by means of moving debris (9). Hyperechoic foci due to microbubbles of gas may be seen within the abscess (19). Organized abscesses may be surrounded by a hyperechoic "halo" (22). US guidance is being used for therapeutic drainage (28,29).

Chronic Sialadenitis

Chronic sialadenitis is clinically characterized by intermittent swelling of the gland, often painful, that may or may not be associated with food (30).

Teaching Point

In chronic inflammation, salivary glands are normal sized or smaller, hypoechoic, and inhomogeneous and usually do not have increased blood flow at US (Fig 14) (9,22,24).

At US, chronic and sometimes acute sialadenitis in children (Fig 13), as well as acalculous submandibular gland sialadenitis in adults, have also been described as showing multiple small, round or oval, hypoechoic areas or lesions distributed throughout glandular parenchyma (23,25,31). The differential diagnosis in such cases includes sarcoidosis and other granulomatous diseases,

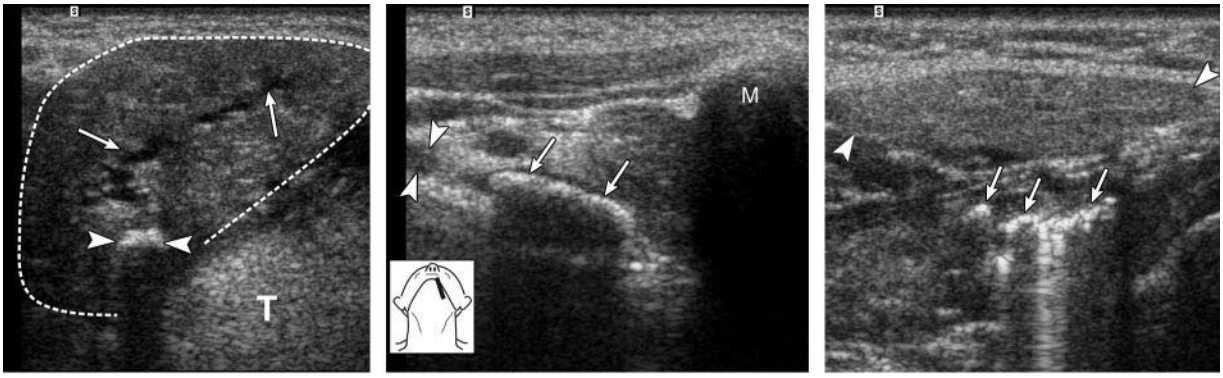

15. 16. 17.

Figures 15–17. **(15)** US image obtained obliquely relative to the mandible shows a sialolith (arrowheads) in the inflamed parenchyma of the right submandibular gland (dashed line), which appears hypoechoic and inhomogeneous. The intraglandular excretory duct (arrows) above the stone is dilated. *T* = tongue. **(16)** US image shows a stone (arrows) in the dilated Wharton duct (arrowheads) near its orifice at the sublingual caruncle. *M* = acoustic shadow behind the surface of the body of the mandible. The position of the US probe is shown in the inset diagram. **(17)** US image shows hyperechoic linear structures (arrows), which may be mistaken for sialoliths in the Wharton duct. These structures represent air bubbles in the oral cavity. Note the "dirty" (not purely anechoic) shadow behind the hyperechoic lines and points. Arrowheads = submandibular gland.

Sjögren syndrome, disseminated lymphoma, hematogenous metastases, and benign lymphoepithelial lesions in human immunodeficiency virus (HIV)–positive patients (32–35).

Chronic Sclerosing Sialadenitis

A special form of chronic sialadenitis that may mimic a malignant lesion, both clinically and at imaging, is chronic sclerosing sialadenitis (Küttner tumor) (36,37). In Küttner tumor, diffuse involvement of the salivary gland (usually the submandibular gland) may occur, with multiple small hypoechoic foci scattered on a heterogeneous background of salivary tissue visible at US (36). Focal involvement may also be encountered, with a focal hypoechoic heterogeneous lesion within a normally shaped gland (36,37). In all doubtful cases, verification with fine-needle aspiration biopsy is recommended (38,39).

Granulomatous Sialadenitis

Granulomatous sialadenitis occurs only rarely (20). US features of granulomatous sialadenitis are nonspecific: single or multiple hypoechoic areas in an enlarged or normally sized gland or diffuse low echogenicity (9,12,19,40–43). Blood flow may be increased (40).

Mycobacterial disease of major salivary glands may manifest as a salivary gland mass, clinically indistinguishable from a neoplasm (44). In the parenchymal type of tuberculosis, Chou et al (45) described focal, intraparotid, nearly anechoic zones that might have a cavity or cavities within them. In necrotic caseous cavities, which appear very hypoechoic, no color flow signals can be detected at US, in contrast to most salivary tumors (45). Salivary gland actinomycosis may mimic a malignant tumor at US; it may manifest as a hypoechoic area with ill-defined margins (46).

Lymph Nodes in Sialadenitis

In acute or chronic inflammation, lymph nodes may be enlarged; however, their normal echostructure (homogeneous cortex and hyperechoic central hilum) is preserved. Central blood vessels or short vessel segments may be visible. Increased central blood flow in lymph nodes may be observed in acute inflammation (26).

Sialolithiasis

Salivary stones are most often located in the submandibular gland (60%–90% of cases) and may be multiple (47–50). Parotid glands are affected in about 10%–20% of cases (51).

On classic radiographs, intraglandular and small stones may be missed, and only about 20% of sialoliths are radiopaque (52). CT allows visualization of large stones but without their precise localization and without the possibility of assessment of the ducts (53). The standard technique for imaging of the submandibular duct and the intraglandular ductal system remains digital sialography (54). A novel, noninvasive, promising method appears to be MR sialography, which also gives very good results in detection of sialoliths (2,54,55). US is a noninvasive method, well-established in cases of clinical suspicion of sialolithiasis, and is used as a primary modality, particularly in Europe (51,54). Although some authors

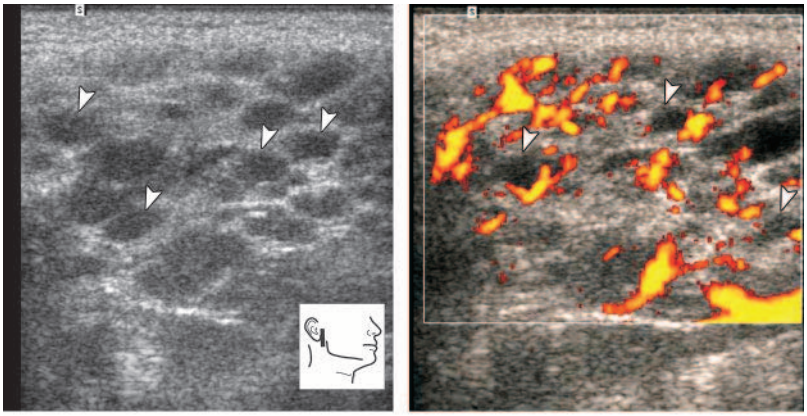

Figure 18. Gray-scale **(a)** and power Doppler **(b)** US images show advanced-stage Sjögren syndrome in the parotid gland. The gland has an inhomogeneous structure with multiple small, oval, hypoechoic areas (arrowheads) and increased blood flow. The position of the US probe is shown in the inset diagram.

claim that sialoliths smaller than 2–3 mm may be overlooked because of the absence of acoustic shadow, these articles are from the 1980s and currently used machines have better resolution and detection possibilities (56,57).

Sialolithiasis causes partial or total mechanical obstruction of the salivary duct, which results in recurrent swelling of a salivary gland during eating and may be complicated by bacterial infection (20,48).

Sialoliths in the distal part of the submandibular duct (Wharton duct) may be palpable in the floor of the mouth. However, sialoliths in the proximal portion of the duct or in the parenchyma of salivary glands may be demonstrated only radiologically.

Teaching Point

US features of sialolithiasis include strongly hyperechoic lines or points with distal acoustic shadowing, which represent stones (Fig 15) (22). In symptomatic cases with duct occlusion, dilated excretory ducts are visible (22).

When sialolithiasis of the submandibular gland is suspected, US may demonstrate whether the stone is located in the glandular parenchyma or in the Wharton duct (Figs 15, 16) (58). This distinction is essential for choosing the method of treatment.

In chronic ductal sialolithiasis complicated by chronic or recurrent inflammation, the gland may lose its function. At this stage of disease, stones located in a nondilated duct may be difficult to demonstrate.

Stones located near the duct orifice or in the middle part of the Wharton duct may sometimes be better demonstrated when additional pressure is administered from inside the oral cavity during US examination.

In about 50% of patients, sialolithiasis coexists with inflammation (23). Hyperechoic bubbles of air mixed with saliva may mimic stones in the Wharton duct and thus be a diagnostic pitfall (Fig 17) (19).

Sialosis

Sialosis is a noninflammatory, nonneoplastic, recurrent, painless salivary gland swelling, usually bilateral, which most often concerns the parotid glands. Sialosis has been described in connection with endocrine diseases, malnutrition, hepatic cirrhosis, chronic alcoholism, or different deficiency diseases (eg, avitaminoses) (20). US reveals enlarged, hyperechoic salivary glands with a poorly visible deep lobe but without focal lesions or increased blood flow (9).

Sjögren Syndrome

Sjögren syndrome is a chronic autoimmune disease predominantly affecting women over 40 years of age. It is characterized by intense lymphocytic and plasma cell infiltration and destruction of salivary and lacrimal glands (59). Major clinical symptoms include a dry mouth and eyes. Advanced stages of Sjögren syndrome may be recognizable at US examination of the parotid and submandibular glands (60). The disease may affect all salivary glands.

US features of advanced Sjögren syndrome include inhomogeneous structure of the gland with scattered multiple small, oval, hypoechoic or anechoic areas, usually well defined, and increased parenchymal blood flow (Fig 18) (9,32,61). Hypoechoic or anechoic areas are believed to represent infiltration by lymphatic cells, destroyed salivary parenchyma, and dilated ducts.

Sjögren syndrome is frequently associated with both reactive and neoplastic lymphoproliferative disease (62). Further US monitoring for early detection of possible lymphomatous change is required in patients with Sjögren syndrome (63,64). Biopsy is recommended for lesions exceeding 2 cm or fast-growing lesions (9). Differential diagnosis of Sjögren syndrome with

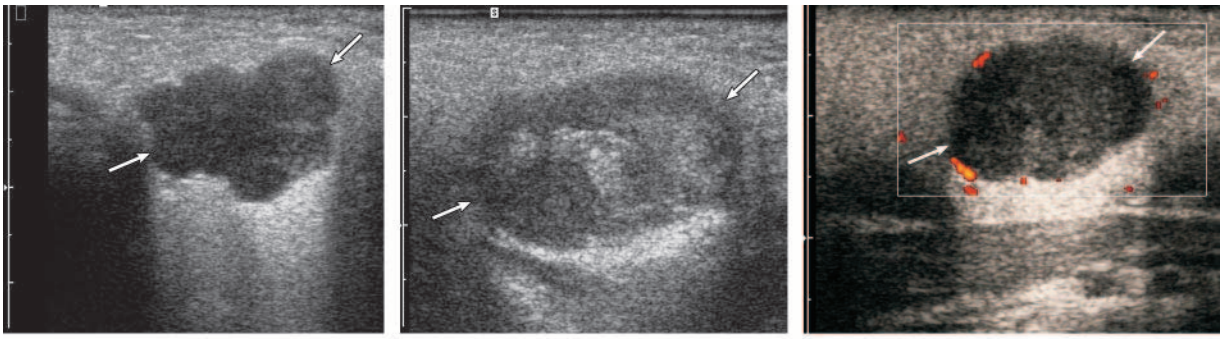

19. 20. 21.

Figures 19–21. **(19)** Gray-scale US image shows the typical appearance of a pleomorphic adenoma (arrows). The lesion is hypoechoic and lobulated with distinct borders and posterior acoustic enhancement. **(20)** US image shows an inhomogeneous pleomorphic adenoma (arrows). **(21)** Power Doppler US image shows a pleomorphic adenoma (arrows) in the lower pole of the parotid gland. No blood vessels are visible in the lesion.

disseminated lymphoma in salivary glands may be challenging. Non-Hodgkin lymphoma manifesting as small multiple nodular disseminations with hypervascularization in the salivary gland has been reported (34,65). In addition, bilateral inflammation (acalculous), granulomatous disease (eg, sarcoidosis), hematogenous metastases, and benign lymphoepithelial lesions in HIV-positive patients should be taken into consideration in cases of multiple hypoechoic areas scattered in salivary gland parenchyma (23,25,33,35,42,43).

Neoplasms

Salivary gland neoplasms are relatively rare. Most of them are benign (70%–80%) and found in the parotid glands (80%–90%). About 10%–12% of all salivary gland neoplasms are located in the submandibular glands, but almost half of these neoplasms may be malignant (3,66).

Benign Neoplasms

Teaching Point

The most common benign neoplasms of major salivary glands are pleomorphic adenomas (mixed tumor) and Warthin tumors (adenolymphoma, cystadenolymphoma, papillary cystadenoma lymphomatosum). Clinically, they manifest as slowly growing painless masses (67). However, small lesions may be detected incidentally at US. When their US appearance is analyzed, many common features may be found, but definitive differential diagnosis is usually not possible with US even between benign and malignant tumors.

Pleomorphic Adenoma.—Pleomorphic adenomas occur most often in the parotid gland (60%–90%) in people in the fourth and fifth decades of life but may arise at any age (3,66,68). There is a slight predominance in women (66). Pleomorphic adenomas are usually solitary and unilateral (3,66,68). They grow slowly and may be asymptomatic.

Nontreated pleomorphic adenomas may undergo malignant transformation after decades (3,68). In exceptional cases, pleomorphic adenomas may be clinically aggressive; they may metastasize and even be fatal (20,69,70).

At US, pleomorphic adenomas are hypoechoic, well-defined, lobulated tumors with posterior acoustic enhancement (Fig 19) and may contain calcifications (71–73). The feature of lobulated shape is being emphasized in differential diagnosis (73).

Many authors add also a feature of homogeneity, but it seems to depend on the composition of the tumor; when high-resolution transducers are used, more and more internal inhomogeneities are being found (Fig 20) (71,73,74).

Vascularization in pleomorphic adenomas is often poor or absent (even when the sensitive power Doppler mode is used) (Fig 21) but may be abundant (71,73,74). After inadequate surgery, pleomorphic adenomas often recur, usually multifocally (75).

Warthin Tumor.—Warthin tumor is the next most common benign salivary neoplasm (5%–10% of all benign salivary neoplasms) (66,68). It arises most often in men in the fifth and sixth decades of life (66,68,76). The relationship between smoking and development of Warthin tumors has been proved (67). Warthin tumor is usually solitary, unilateral, and slow growing. In about 10%–

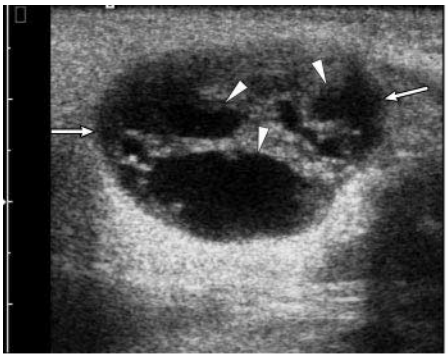

22.

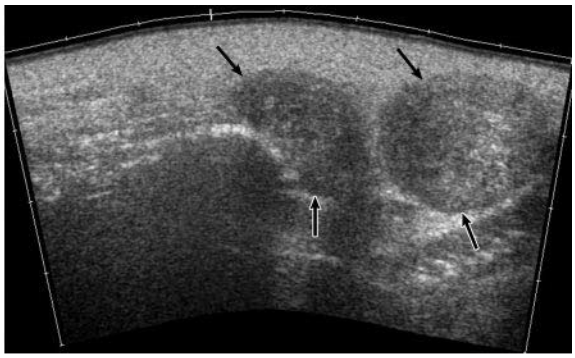

23.

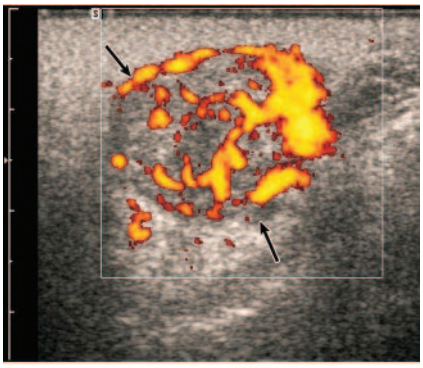

24.

Figures 22–24. **(22)** Gray-scale US image shows the typical appearance of a Warthin tumor (arrows). The lesion, which is located in the lower pole of the parotid gland, is oval, well defined, hypoechoic, and inhomogeneous with multiple irregular anechoic areas (arrowheads) and posterior acoustic enhancement. **(23)** Panoramic gray-scale US image shows two Warthin tumors (arrows) in the lower pole of the left parotid gland. The lesions are oval, well defined, hypoechoic, and inhomogeneous. **(24)** Power Doppler US image shows a hypervascularized Warthin tumor (arrows) in the parotid gland.

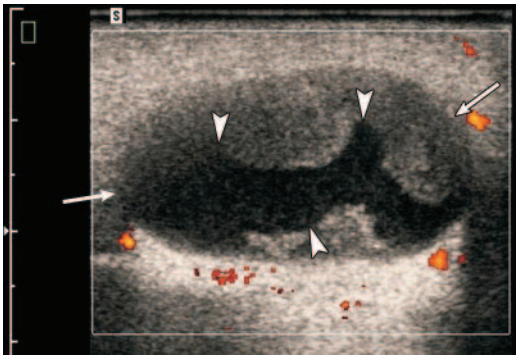

Figure 25. US image shows a pleomorphic adenoma (arrows) with an anechoic area (arrowheads), an appearance that mimics a Warthin tumor.

60% of cases, tumors may occur bilaterally or multifocally, sometimes metachronously, growing and manifesting clinically at different times (3,68,77,78). Sporadically, the epithelial component of Warthin tumor may undergo malignant transformation (68,79).

At US, Warthin tumors are oval, hypoechoic, well-defined tumors and often contain multiple anechoic areas (Figs 22, 23) (25,74,78,80). Warthin tumors are often hypervascularized (Fig 24) but may also contain only short vessel segments.

Diagnosis of a Warthin tumor may be supported by results of technetium 99m scintigraphy, which reveals a "hot" tumor because of the increased uptake of the tracer by the tumor (81). However, some other parotid neoplasms, benign as well as malignant, may sporadically show uptake of the radionuclide.

Lobulated shape in pleomorphic adenomas and anechoic areas in Warthin tumors, although common, are not pathognomonic and may be found in many other lesions, including malignancies (73,74) (Fig 25). For example, macroscopic cystic structures, which appear as anechoic areas at US, may occur in other benign tumors (pleomorphic adenoma, basal cell adenoma), in malignant tumors (mucoepidermoid carcinoma, acinic cell carcinoma), and in an abscessed or necrotic metastatic node; in addition, benign lymphoepithelial lesions in HIV-positive patients may have the appearance of solid-cystic nodules (Fig 25) (3,35,72,74,82–86). Warthin tumor may also appear in the form of a simple cyst at US and thus require differentiation from cystic carcinomas (mucoepidermoid carcinoma, acinic cell carcinoma) and benign cysts (lymphoepithelial cysts) (43,73,82).

Other Benign Tumors.—Other benign tumors (eg, oncocytoma, basal cell adenoma) occur less frequently in the salivary glands. Their differentiation is not possible with US. Among nonepithelial lesions, hemangiomas, lipomas (Fig 26), and neurinomas or schwannomas may be found in salivary glands (12,87–91).

Hemangiomas, the most frequent tumors in infants, may manifest as heterogeneous lesions with sinusoidal spaces and calcifications representing phleboliths (88). Lipomas are usually oval and hypoechoic with sharp margins and hyperechoic linear structures regularly distributed within the lesion in a striated or feathered pattern (Fig 26) (9,92). At color or power Doppler US, only single vessel segments may be found (9). In infants with hemangioma, US may show a homogeneous, mildly lobulated mass with a lobular structure, fine echogenic septa, and extremely high vascularization at color Doppler imaging (93). Other vascular lesions, such as pseudoaneurysms or arteriovenous fistulas, may also be encountered in the parotid gland, although they are rare (88). Neurogenic tumors often contain anechoic areas (25).

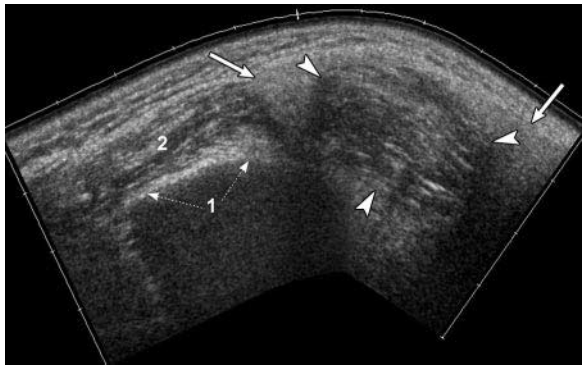

Figure 26. Panoramic gray-scale US image shows the typical appearance of a lipoma (arrowheads). The lesion, which is located in the left parotid gland (arrows), is hypoechoic with regularly distributed linear structures. *1* = echo from the surface of the ramus of the mandible, *2* = masseter muscle.

Malignant Neoplasms

The most common malignant neoplasms occurring in salivary glands are mucoepidermoid carcinoma and adenoid cystic carcinoma (94). Squamous cell carcinoma, acinic cell carcinoma, and adenocarcinoma are less common. Less than 30% of focal lesions in the parotid gland are malignant, whereas almost 50% of focal lesions in the submandibular gland are malignant (3,66).

Unlike benign salivary neoplasms, malignant tumors may grow rapidly, may be tender or painful at palpation, may be fixed to the background, and may cause facial nerve paresis or paralysis (3,20,94).

Mucoepidermoid carcinoma occurs mostly between 30 and 50 years of age. Mucoepidermoid carcinoma may show several levels of differentiation and thus different tendencies to infiltration, metastases, and progress; the poorly differentiated form is extremely aggressive (20). The macroscopic appearance of the tumor, and similarly its imaging features, depend mostly on the level of malignancy (8,20). Well-differentiated tumors may be similar to benign tumors at US (8). Adenoid cystic carcinoma, which is a slowly growing tumor, shows a particular tendency to nerve infiltration (and thus pain), and late metastases are frequent (20).

Classic US features of poorly differentiated or advanced malignant neoplasms of salivary glands are like those in other organs or tissues. US features of malignant salivary neoplasms include the following: an irregular shape, irregular borders, blurred margins, and a hypoechoic inhomogeneous structure (Figs 27, 28) (8,19,25,41,95,96). However, malignant tumors may also be homogeneous and well defined (18,73,96). The internal structure of a malignant tumor at US may be not only solid but also cystic or cystic with a mural solid nodule (85). Malignant tumors may have a lobulated shape, similar to that of pleomorphic adenomas (96).

Vascularization of malignant tumors is not pathognomonic, and assessment with color Doppler or power Doppler US does not allow reliable differentiation between benign and malignant salivary gland tumors (72,76). However, Schick et al (72) report that high vascularization and high systolic peak flow velocity should raise the suspicion of malignancy. On the other hand, Bradley et al (97) conclude that tumors demonstrating an increased intratumoral vascular resistance index have an increased risk of malignancy.

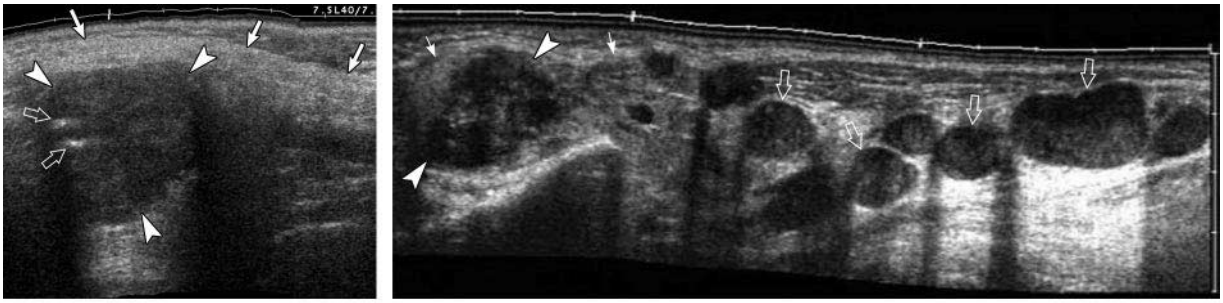

27. 28.

Figures 27, 28. **(27)** Panoramic gray-scale US image shows an acinic cell carcinoma (arrowheads) in the left parotid gland (solid arrows). The tumor is well defined and has regular margins; however, there are signs of mandibular destruction (open arrows), a finding that suggests malignancy. **(28)** Panoramic gray-scale US image shows metastatic lymph nodes (open arrows), which are oval or round and inhomogeneous without hyperechoic hila. There is a primary adenocarcinoma (arrowheads) in the left parotid gland (solid arrows).

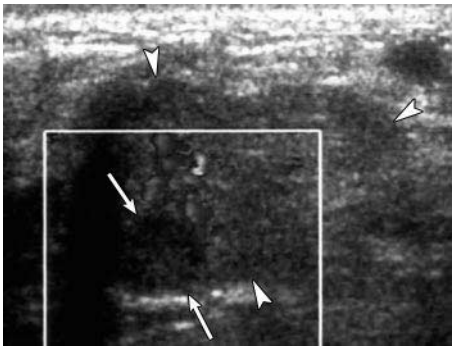

Figure 29. US image shows an oval, well-defined, homogeneous tumor with even margins (arrows) in the right submandibular gland; the parenchyma of the gland (arrowheads) has been changed by therapeutic neck irradiation. Despite its benign features, the tumor proved to be a metastasis from a squamous cell carcinoma at the base of the tongue.

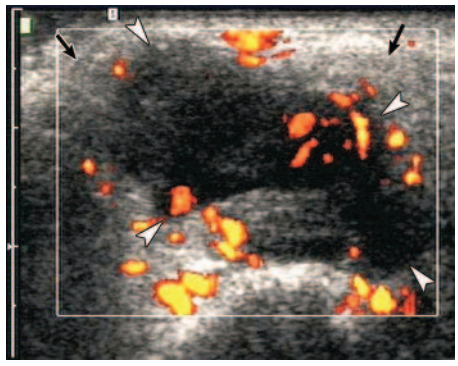

Figure 30. Power Doppler US image shows a metastasis (arrowheads) to the superficial lobe of the parotid gland (arrows) from a melanoma. The tumor is lobulated, inhomogeneous, and virtually anechoic with posterior acoustic enhancement and chaotic, mainly peripheral vessel segments.

The presence of metastatic-appearing lymph nodes accompanying a tumor in the salivary gland strongly suggests a malignancy (Fig 28). Very rarely, malignant tumors may occur multifocally or bilaterally, sometimes metachronously, or may coexist with benign neoplasms (78,96,98).

An important problem in US is caused by small malignant neoplasms and metastases, less than 20 mm in diameter, and well-differentiated malignant neoplasms because they may demonstrate benign features: clear, even margins and homogeneous structure (Fig 29) (72,73). These tumors also cause similar diagnostic problems with other diagnostic methods (CT and MR imaging) (3).

Metastases

Salivary glands are very uncommonly sites of metastases. Primary tumors metastasizing to salivary glands may be located in the head and neck region, as well as in more distant parts of the body. Melanoma (Fig 30), spinocellular cancer, breast cancer, and lung cancer may produce metastases to intraparotid lymph nodes (99–103). Extremely rare are metastases from renal cancer (100,104–106).

At US, metastases may be well defined and oval (Fig 29) (9). It may be difficult to differentiate multiple metastatic lesions from some

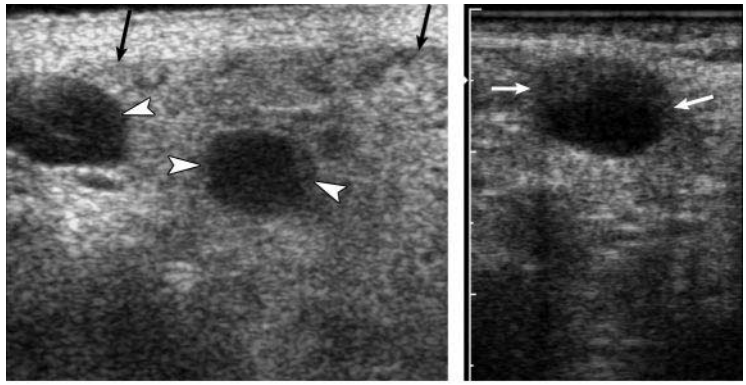

Figures 31, 32. **(31)** US image of a patient with follicular lymphoma shows affected lymph nodes (arrowheads) in the parotid gland (arrows = external outline of the superficial lobe). Affected nodes were also located beneath and along the sternocleidomastoid muscle. **(32)** Gray-scale US image of a patient with non-Hodgkin lymphoma shows a lymphomatous lymph node (arrows) in the parotid gland. The oval, well-defined, anechoic lesion demonstrates discrete posterior enhancement and mimics a simple cyst.

patterns of inflammation, Sjögren syndrome, and granulomatous disease at US (23,25,33,42,43).

Lymphoma

Salivary glands may also be affected by lymphoma (Fig 31) (34). However, primary involvement of salivary glands is rare; they are usually one of the sites of systemic disease. Clinically, salivary lymphomas most often manifest as a painless, progressive swelling (107,108). They are usually associated with autoimmune disease, most often with Sjögren syndrome, sometimes also with rheumatoid arthritis (62–64,109).

At US of cases of lymphoma in the salivary gland, one may observe a solitary, hypoechoic, homogeneous or inhomogeneous lesion, which is oval or lobulated or has irregular margins and sometimes contains echogenic septa or stripes (34,110,111). However, these features are not pathognomonic, and lymphoma may not be reliably differentiated from other neoplastic or nonneoplastic salivary gland tumors with US. A pattern of multiple hypoechoic lesions with increased blood flow may also be seen (34,111). Such a pattern requires differentiation from inflammation, Sjögren syndrome, granulomatous disease (eg, sarcoidosis), and hematogenous metastases (23,25,32,33,42,43). In cases of lymphoma, solitary or multiple salivary gland lesions sometimes associated with microcysts may be observed at CT or MR imaging (63,109).

Multiple lesions simulating Sjögren syndrome may also be difficult to diagnose with other imaging methods (eg, MR imaging) (109). At gray-scale US, lymphomatous lymph nodes may demonstrate all the US features of a simple cyst (Fig 32) (112,113).

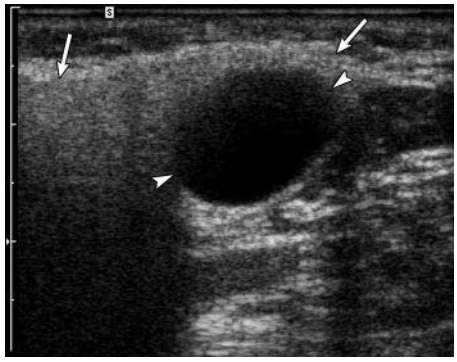

Figure 33. Gray-scale tissue harmonic US image shows a simple cyst (arrowheads) in the lower pole of the parotid gland (arrows).

Cysts

Simple cysts are uncommon in salivary glands. They may be congenital or acquired. Some acquired cysts develop due to obstruction of the salivary ducts in the presence of a tumor, stones, or inflammation (3). Clinically, they usually manifest as a painless swelling but may be tender when infected (41).

Teaching Point

US features of a cyst are classic (like in any other location in the body): well-defined margins, anechoic content, posterior acoustic enhancement, and no evidence of internal blood flow at power Doppler or color Doppler imaging (Fig 33) (22).

Benign lymphoepithelial lesions in HIV-positive patients may manifest as multiple cysts (35).

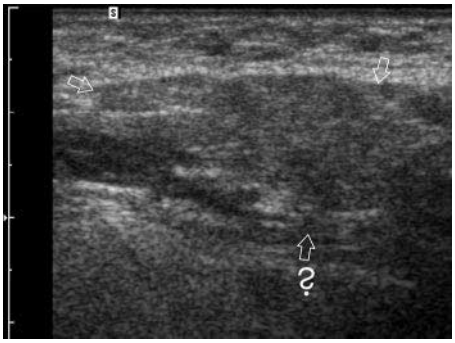

Figure 34. US image shows the left submandibular gland (arrows) 9 years after therapeutic irradiation of the neck. The gland is hypoechoic and inhomogeneous, contains separate hyperechoic linear structures, and has partially irregular and difficult to follow outlines. *?* = equivocal lower margin of the submandibular gland.

Possible diagnostic pitfalls include a "pseudocystic" appearance of lymphoma, the cystic form of Warthin tumor, lymphoepithelial lesions, or metastatic lymph nodes with a central fluid collection or necrosis (35,43,73,82,112–114).

Effects of Irradiation

The major salivary glands are often irradiated during radiation therapy of head and neck neoplasms. A major adverse effect of such treatment is xerostomia caused by functional and structural impairment of salivary parenchyma (11,115). Loss of salivary gland function significantly diminishes the patient's quality of life (116). The most useful method for evaluation of salivary excretory function remains scintigraphy, especially single photon emission CT (SPECT) (10,11). Carbon 11–methionine positron emission tomography (PET) offers new possibilities for studying the individual response of major salivary glands to irradiation (117). After irradiation, salivary glands become hypoechoic and inhomogeneous at US (Fig 34). The salivary glands enlarge in the acute phase and later become smaller because of atrophy (19,118,119). Postirradiation edema corresponding to sialadenitis is well visible on T2-weighted MR images (119).

Trauma

Traumatic injuries of the salivary glands occur most often in the parotid gland because the other major salivary glands are protected by the mandible. After salivary gland trauma, US may demonstrate a hematoma, other fluid collections (eg, a sialocele), or a fistula in the parotid gland or surrounding structures (13,19,120,121). Suspected damage to the facial nerve or Stenon duct warrants application of other imaging modalities (CT, MR, sialography) (19).

Conclusions

US is a valuable and useful method for diagnosis of salivary gland diseases. Not only does it enable confirmation or exclusion of the presence of a mass, but in many cases the nature of underlying disease may also be suggested on the basis of US findings.

References

1. Rabinov JD. Imaging of salivary gland pathology. Radiol Clin North Am 2000;38:1047–1057.
2. Yousem DM, Kraut MA, Chalian AA. Major salivary gland imaging. Radiology 2000;216:19–29.
3. Silvers AR, Som PM. Salivary glands. Radiol Clin North Am 1998;36:941–966.
4. Alyas F, Lewis K, Williams M, et al. Diseases of the submandibular gland as demonstrated using high resolution ultrasound. Br J Radiol 2005;78:362–369.
5. Ridder GJ, Richter B, Disko U, Sander A. Grayscale sonographic evaluation of cervical lymphadenopathy in cat-scratch disease. J Clin Ultrasound 2001;29:140–145.
6. Ying M, Ahuja A, Metreweli C. Diagnostic accuracy of sonographic criteria for evaluation of cervical lymphadenopathy. J Ultrasound Med 1998;17:437–445.
7. Ying M, Ahuja A. Sonography of neck lymph nodes. I. Normal lymph nodes. Clin Radiol 2003;58:351–358.
8. Howlett DC, Kesse KW, Hughes DV, Sallomi DF. The role of imaging in the evaluation of parotid disease. Clin Radiol 2002;57:692–701.
9. Gritzmann N, Rettenbacher T, Hollerweger A, Macheiner P, Hubner E. Sonography of the salivary glands. Eur Radiol 2003;13:964–975.
10. Bussels B, Maes A, Flamen P, et al. Dose-response relationships within the parotid gland after radiotherapy for head and neck cancer. Radiother Oncol 2004;73:297–306.
11. Roesink JM, Moerland MA, Hoekstra A, Van Rijk PP, Terhaard CH. Scintigraphic assessment of early and late parotid gland function after radiotherapy for head-and-neck cancer: a prospective study of dose-volume response relationships. Int J Radiat Oncol Biol Phys 2004;58:1451–1460.
12. Koischwitz D, Gritzmann N. Ultrasound of the neck. Radiol Clin North Am 2000;38:1029–1045.

13. Candiani F, Martinoli C. Salivary glands. In: Solbiati L, Rizzatto G, eds. Ultrasound of superficial structures. Edinburgh, Scotland: Churchill Livingstone, 1995; 125–139.
14. Thoron JF, Rafaelli C, Carlotti B, et al. Ultrasonography of the parotid venous plane [in French]. J Radiol 1996;77:667–669.
15. Takahashi N, Okamoto K, Ohkubo M, Kawana M. High-resolution magnetic resonance of the extracranial facial nerve and parotid duct: demonstration of the branches of the intraparotid facial nerve and its relation to parotid tumours by MRI with a surface coil. Clin Radiol 2005;60: 349–354.
16. Divi V, Fatt MA, Teknos TN, Mukherji SK. Use of cross-sectional imaging in predicting surgical location of parotid neoplasms. J Comput Assist Tomogr 2005;29:315–319.
17. Lin DT, Coppit GL, Burkey BB, Netterville JL. Tumors of the accessory lobe of the parotid gland: a 10-year experience. Laryngoscope 2004; 114:1652–1655.
18. Yoshihara T, Suzuki S, Nagao K. Mucoepidermoid carcinoma arising in the accessory parotid gland. Int J Pediatr Otorhinolaryngol 1999;48: 47–52.
19. Bradley MJ. Salivary glands. In: Ahuja AT, Evans RM, eds. Practical head and neck ultrasound. London, England: Greenwich Medical Media, 2000; 19–33.
20. Sikorowa L, Meyza JW, Ackerman LW. Salivary gland tumors. New York, NY: Pergamon, 1982.
21. Brook I. Acute bacterial suppurative parotitis: microbiology and management. J Craniofac Surg 2003;14:37–40.
22. Traxler M, Schurawitzki H, Ulm C, et al. Sonography of nonneoplastic disorders of the salivary glands. Int J Oral Maxillofac Surg 1992;21:360–363.
23. Ching AS, Ahuja AT, King AD, Tse GM, Metreveli C. Comparison of the sonographic features of acalculous and calculous submandibular sialadenitis. J Clin Ultrasound 2001;29:332–338.
24. Garcia CJ, Flores PA, Arce JD, Chuaqui B, Schwartz DS. Ultrasonography in the study of salivary gland lesions in children. Pediatr Radiol 1998;28:418–425.
25. Shimizu M, Ussmüller J, Donath K, et al. Sonographic analysis of recurrent parotitis in children: a comparative study with sialographic findings. Oral Surg Oral Med Oral Pathol Oral Radiol Endod 1998;86:606–615.
26. Tschammler A, Ott G, Schang T, Seelbach-Goebel B, Schwager K, Hahn D. Lymphadenopathy: differentiation of benign from malignant disease—color Doppler US assessment of intranodal angioarchitecture. Radiology 1998; 208:117–123.
27. Duff TB. Parotitis, parotid abscess and facial palsy. J Laryngol Otol 1972;86:161–165.
28. Thiede O, Stoll W, Schmal F. Clinical aspects of abscess development in parotitis [in German]. HNO 2002;50:332–338.
29. Yeow KM, Hao SP, Liao CT. US-guided percutaneous catheter drainage of parotid abscesses. J Vasc Interv Radiol 2000;11:473–476.
30. Bhatty MA, Piggot TA, Soames JV, McLean NR. Chronic non-specific parotid sialadenitis. Br J Plast Surg 1998;51:517–521.
31. Nozaki H, Harasawa A, Hara H, Kohno A, Shigeta A. Ultrasonographic features of recurrent parotitis in childhood. Pediatr Radiol 1994;24: 98–100.
32. Steiner E, Graninger W, Hitzelhammer J, et al. Color-coded duplex sonography of the parotid gland in Sjogren's syndrome [in German]. Rofo 1994;160:294–298.
33. Gnepp DR. Metastatic disease to the major salivary glands. In: Ellis GL, Auclair PL, Gnepp DR, eds. Surgical pathology of the salivary glands. Philadelphia, Pa: Saunders, 1991; 560.
34. Chiou HJ, Chou YH, Chiou SY, et al. High-resolution ultrasonography of primary peripheral soft tissue lymphoma. J Ultrasound Med 2005;24: 77–86.
35. Martinoli C, Pretolesi F, Del Bono V, Derchi LE, Mecca D, Chiaramondia M. Benign lymphoepithelial parotid lesions in HIV-positive patients: spectrum of findings at gray-scale and Doppler sonography. AJR Am J Roentgenol 1995;165:975–979.
36. Ahuja AT, Richards PS, Wong KT, et al. Kuttner tumour (chronic sclerosing sialadenitis) of the submandibular gland: sonographic appearances. Ultrasound Med Biol 2003;29:913–919.
37. Bialek EJ, Osmólski A, Karpinska G, et al. US-appearance of a Küttner tumor resembling a malignant lesion: US-histopathologic correlation. Eur J Ultrasound 2001;14:167–170.
38. Siewert B, Kruskal JB, Kelly D, Sosna J, Kane RA. Utility and safety of ultrasound-guided fine-needle aspiration of salivary gland masses including a cytologist's review. J Ultrasound Med 2004; 23:777–783.
39. Wan YL, Chan SC, Chen YL, et al. Ultrasonography-guided core-needle biopsy of parotid gland masses. AJNR Am J Neuroradiol 2004;25:1608–1612.
40. Fischer T, Muhler M, Beyersdorff D, et al. Use of state-of-the-art ultrasound techniques in diagnosing sarcoidosis of the salivary glands (Heerfordt's syndrome) [in German]. HNO 2003;51: 394–399.
41. Howlett DC. High resolution ultrasound assessment of the parotid gland. Br J Radiol 2003;76: 271–277.
42. Iko BO, Chinwuba CE, Myers EM, Teal JS. Sarcoidosis of the parotid gland. Br J Radiol 1986; 59:547–552.

43. Martinoli C, Derchi LE, Solbiati L, Rizzatto G, Silvestri E, Giannoni M. Color Doppler sonography of salivary glands. AJR Am J Roentgenol 1994;163:933–941.
44. Holmes S, Gleeson MJ, Cawson RA. Mycobacterial disease of the parotid gland. Oral Surg Oral Med Oral Pathol Oral Radiol Endod 2000;90: 292–298.
45. Chou YH, Tiu CM, Liu CY, et al. Tuberculosis of the parotid gland: sonographic manifestations and sonographically guided aspiration. J Ultrasound Med 2004;23:1275–1281.
46. Sa'do B, Yoshiura K, Yuasa K, et al. Multimodality imaging of cervicofacial actinomycosis. Oral Surg Oral Med Oral Pathol 1993;76:772–782.
47. Escudier MP, McGurk M. Symptomatic sialadenitis and sialolithiasis in the English population: an estimate of the cost of hospital treatment. Br Dent J 1999;186:463–466.
48. Lustmann J, Regev E, Melamed Y. Sialolithiasis: a survey on 245 patients and a review of the literature. Int J Oral Maxillofac Surg 1990;19:135–138.
49. Marchal F, Dulgerov P, Becker M, Barki G, Disant F, Lehmann W. Specificity of parotid sialendoscopy. Laryngoscope 2001;111:264–271.
50. Marchal F, Dulgerov P, Becker M, Barki G, Disant F, Lehmann W. Submandibular diagnostic and interventional sialendoscopy: new procedure for ductal disorders. Ann Otol Rhinol Laryngol 2002;111:27–35.
51. Zenk J, Constantinidis J, Kydles S, Hornung J, Iro H. Clinical and diagnostic findings of sialolithiasis [in German]. HNO 1999;47:963–969.
52. Rauch S, Gorlin RJ. Disease of the salivary glands. In: Gorlin RJ, Goldmann HM, eds. Thomas' oral pathology. St Louis, Mo: Mosby, 1970; 997–103.
53. Avrahami E, Englender M, Chen E, Shabaty D, Katz R, Harell M. CT of submandibular gland sialolithiasis. Neuroradiology 1996;38:287–290.
54. Jäger L, Menauer F, Holzknecht N, Scholz V, Grevers G, Reiser M. Sialolithiasis: MR sialography of the submandibular duct—an alternative to conventional sialography and US? Radiology 2000;216:665–671.
55. Becker M, Marchal F, Becker CD, et al. Sialolithiasis and salivary ductal stenosis: diagnostic accuracy of MR sialography with a three-dimensional extended-phase conjugate-symmetry rapid spin-echo sequence. Radiology 2000;217:347–358.
56. Diederich S, Wernecke K, Peters PE. Sialographic and sonographic diagnosis of diseases of the salivary gland [in German]. Radiologe 1987; 27:255–261.
57. Rinast E, Gmelin E, Hollands-Thorn B. Digital subtraction sialography, conventional sialography, high-resolution ultrasonography and computed tomography in the diagnosis of salivary gland diseases. Eur J Radiol 1989;9:224–230.
58. Gritzmann N, Hajek P, Karnel F, Fezoulidis J, Türk R. Sonography in salivary calculi: indications and status [in German]. Rofo 1985;142: 559–562.
59. Kumar V, Cotran RS, Robbins SL. Disorders of the immune system. In: Basic pathology. 6th ed. Philadelphia, Pa: Saunders, 1997; 111–112.
60. Makula É, Pokorny G, Kiss M, et al. The place of magnetic resonance and ultrasonographic examinations of the parotid gland in the diagnosis and follow-up of primary Sjögren syndrome. Rheumatology (Oxford) 2000;39:97–104.
61. Niemela RK, Takalo R, Paakko E, et al. Ultrasonography of salivary glands in primary Sjogren's syndrome: a comparison with magnetic resonance imaging and magnetic resonance sialography of parotid glands. Rheumatology (Oxford) 2004;43:875–879.
62. McCurley TL, Collins RD, Ball E, Collins RD. Nodal and extranodal lymphoproliferative disorders in Sjogren's syndrome: a clinical and immunopathologic study. Hum Pathol 1990;21:482–492.
63. Tonami H, Matoba M, Kuginuki Y, et al. Clinical and imaging findings of lymphoma in patients with Sjögren syndrome. J Comput Assist Tomogr 2003;27:517–524.
64. Masaki Y, Sugai S. Lymphoproliferative disorders in Sjogren's syndrome. Autoimmun Rev 2004;3:175–182.
65. Matsushita T, Takashima S, Takayama F, Momose M, Wang J, Ishiyama T. Sonographic detection of secondary MALT lymphoma of the submandibular gland. J Clin Ultrasound 2001; 29(8):462–465.
66. Renehan A, Gleave EN, Hancock BD, Smith P, McGurk M. Long-term follow-up of over 1000 patients with salivary gland tumours treated in a single centre. Br J Surg 1996;83:1750–1754.
67. Yoo GH, Eisele DW, Askin FB, Driben JS, Johns ME. Warthin's tumor: a 40-year experience at the Johns Hopkins Hospital. Laryngoscope 1994; 104:799–803.
68. Ellis GL, Auclair PL, Gnepp DR, eds. Surgical pathology of the salivary glands. Philadelphia, Pa: Saunders, 1991.
69. Joe VQ, Westesson PL. Tumors of the parotid gland: MR imaging characteristics of various histologic types. AJR Am J Roentgenol 1994;163: 433–438.
70. Klijanienko J, El-Naggar AK, Servois V, Rodriguez J, Validire P, Vielh P. Clinically aggressive metastasizing pleomorphic adenoma: report of two cases. Head Neck 1997;19:629–633.

71. Bialek EJ, Jakubowski W, Karpinska G. Role of ultrasonography in diagnosis and differentiation of pleomorphic adenomas: work in progress. Arch Otolaryngol Head Neck Surg 2003;129: 929–933.
72. Schick S, Steiner E, Gahleitner A, et al. Differentiation of benign and malignant tumors of the parotid gland: value of pulsed Doppler and color Doppler sonography. Eur Radiol 1998;8:1462–1467.
73. Shimizu M, Ussmüller J, Hartwein J, Donath K, Kinukawa N. Statistical study for sonographic differential diagnosis of tumorous lesions in the parotid gland. Oral Surg Oral Med Oral Pathol Oral Radiol Endod 1999;88:226–233.
74. Zajkowski P, Jakubowski W, Białek EJ, Wysocki M, Osmólski A, Serafin-Król M. Pleomorphic adenoma and adenolymphoma in ultrasonography. Eur J Ultrasound 2000;12:23–29.
75. Laskawi R, Schott T, Schröder M. Recurrent pleomorphic adenomas of the parotid gland: clinical evaluation and long-term follow-up. Br J Oral Maxillofac Surg 1998;36:48–51.
76. Schade G, Ussmuller J, Leuwer R. Stellenwert der duplexsonographie bei der diagnostik von parotistumoren. Laryngorhinootologie 1998;77: 337–341.
77. Gritzmann N, Türk R, Wittich G, Karnel F, Schurawitzki H, Brunner E. High-resolution sonography after surgery of cystadenoma lymphomatosum of the parotid gland [in German]. Rofo 1986;145:648–651.
78. Yu GY, Ma DQ, Zhang Y, et al. Multiple primary tumours of the parotid gland. Int J Oral Maxillofac Surg 2004;33:531–534.
79. Podlešák T, Dolecková V, Sibl O. Malignancy of a cystadenolymphoma of the parotid gland. Eur Arch Otorhinolaryngol 1992;249:233–235.
80. Kim J, Kim EK, Park CS, Choi YS, Kim YH, Choi EC. Characteristic sonographic findings of Warthin's tumor in the parotid gland. J Clin Ultrasound 2004;32:78–81.
81. Canbay AE, Knorz S, Heimann KD, Hildmann H, Tiedjen KU. Sonography and scintigraphy in the diagnosis of cystadenolymphomas (Warthin tumor) [in German]. Laryngorhinootologie 2002;81:815–819.
82. Auclair PL, Ellis GL. Mucoepidermoid carcinoma. In: Ellis GL, Auclair PL, Gnepp DR, eds. Surgical pathology of the salivary glands. Philadelphia, Pa: Saunders, 1991; 269–298.
83. Khadaroo RG, Walton JM, Ramsay JA, Hicks MJ, Archibald SC. Mucoepidermoid carcinoma of the parotid gland: a rare presentation in a young child. J Pediatr Surg 1998;33:893–895.
84. Nishimura T, Furukawa M, Kawahara E. Pleomorphic adenoma of parotid gland with cystic degeneration. J Laryngol Otol 1994;108:446–448.
85. Suh SI, Seol HY, Kim TK, et al. Acinic cell carcinoma of the head and neck: radiologic-pathologic correlation. J Comput Assist Tomogr 2005; 29:121–126.
86. Takeshita T, Tanaka H, Harasawa A, Kaminaga T, Imamura T, Furui S. Benign pleomorphic adenoma with extensive cystic degeneration: unusual MR findings in two cases. Radiat Med 2004;22:357–361.
87. Gritzmann N, Macheiner P. Lipoma in the parotid gland: typical US and CT morphology [in German]. Ultraschall Med 2003;24:195–196.
88. Wong KT, Ahuja AT, King AD, Yuen EH, Yu SC. Vascular lesions of parotid gland in adult patients: diagnosis with high-resolution ultrasound and MRI. Br J Radiol 2004;77:600–606.
89. Chong KW, Chung YF, Khoo ML, Lim DT, Hong GS, Soo KC. Management of intraparotid facial nerve schwannomas. Aust N Z J Surg 2000; 70:732–734.
90. Hehar SS, Dugar J, Sharp J. The changing faces of a parotid mass. J Laryngol Otol 1999;113: 938–941.
91. Oncel S, Onal K, Ermete M, Uluc E. Schwannoma (neurilemmoma) of the facial nerve presenting as a parotid mass. J Laryngol Otol 2002; 116:642–643.
92. Chikui T, Yonetsu K, Yoshiura K, et al. Imaging findings of lipomas in the orofacial region with CT, US, and MRI. Oral Surg Oral Med Oral Pathol Oral Radiol Endod 1997;84:88–95.
93. Roebuck DJ, Ahuja AT. Hemangioendothelioma of the parotid gland in infants: sonography and correlative MR imaging. AJNR Am J Neuroradiol 2000;21:219–223.
94. Paris J, Coulet O, Facon F, Chrestian MA, Giovanni A, Zanaret M. Primary cancer of the parotid gland: an anatomoclinical approach [in French]. Rev Stomatol Chir Maxillofac 2004; 105:309–315.
95. Goto TK, Yoshiura K, Nakayama E, et al. The combined use of US and MR imaging for the diagnosis of masses in the parotid region. Acta Radiol 2001;42:88–95.
96. Hardee PS, Carter JL, Piper KM, Ng SY. Metachronous bilateral primary adenocarcinoma of

the submandibular glands. Oral Surg Oral Med Oral Pathol Oral Radiol Endod 2001;91:455–461.
97. Bradley MJ, Durham LH, Lancer JM. The role of colour flow Doppler in the investigation of the salivary gland tumour. Clin Radiol 2000;55:759–762.
98. Eneroth CM, Hamberger CA, Jakobsson PA. Malignancy of acinic cell carcinoma. Ann Otol Rhinol Laryngol 1966;75:780–792.
99. Dequanter D, Lothaire P, Andry G. Secondary malignant tumors of the parotid [in French]. Ann Otolaryngol Chir Cervicofac 2005;122:18–20.
100. Malata CM, Camilleri IG, McLean NR, Piggott TA, Soames JV. Metastatic tumours of the parotid gland. Br J Oral Maxillofac Surg 1998;36:190–195.
101. Pisani P, Krengli M, Ramponi A, Guglielmetti R, Pia F. Metastases to parotid gland from cancers of the upper airway and digestive tract. Br J Oral Maxillofac Surg 1998;36:54–57.
102. Raut V, Sinnathuray AR, Primrose WJ. Aggressive treatment of metastasis to the parotid. Ulster Med J 2004;73:85–88.
103. Seifert G, Hennign SK, Caselitz J. Metastatic tumours to the parotid and submandibular glands. Pathol Res Pract 1986;181:684–694.
104. Gogus C, Kilic O, Tulunay O, Tulunay O, Beduk Y. Solitary metastasis of renal cell carcinoma to the parotid gland 10 years after radical nephrectomy. Int J Urol 2004;11:894–896.
105. Park YW, Hlivko TJ. Parotid gland metastasis from renal cell carcinoma. Laryngoscope 2002;112:453–456.
106. Seijas BP, Franco FL, Sastre RM, Garcia AA, Lopez-Cedrun Cembranos JL. Metastatic renal cell carcinoma presenting as a parotid tumor. Oral Surg Oral Med Oral Pathol Oral Radiol Endod 2005;99:554–557.
107. Dunn P, Kuo TT, Shih LY, et al. Primary salivary gland lymphoma: a clinicopathologic study of 23 cases in Taiwan. Acta Haematol 2004;112:203–208.
108. Tiplady CW, Taylor PR, White J, Arullendran P, Proctor SJ. Lymphoma presenting as a parotid tumour: a population-based study of diagnosis, treatment and outcome on behalf of the Scotland and Newcastle Lymphoma Group. Clin Oncol (R Coll Radiol) 2004;16:414–419.
109. Rodallec M, Guermazi A, Brice P, et al. Imaging of MALT lymphomas. Eur Radiol 2002;12:348–356.
110. Eichhorn KW, Arapakis I, Ridder GJ. Malignant non-Hodgkin's lymphoma mimicking a benign parotid tumor: sonographic findings. J Clin Ultrasound 2002;30:42–44.
111. Yasumoto M, Yoshimura R, Sunaba K, Shibuya H. Sonographic appearances of malignant lymphoma of the salivary glands. J Clin Ultrasound 2001;29:491–498.
112. Ahuja AT, Ying M, Yuen YH, Metreveli C. "Pseudocystic" appearance of non-Hodgkin's lymphomatous nodes: an infrequent finding with high-resolution transducers. Clin Radiol 2001;56:111–115.
113. Giovagnorio F, Galluzzo M, Andreoli C, De Cicco ML, David V. Color Doppler sonography in the evaluation of superficial lymphomatous lymph nodes. J Ultrasound Med 2002;21:403–408.
114. Kessler A, Rappaport Y, Blank A, Marmor S, Weiss J, Graif M. Cystic appearance of cervical lymph nodes is characteristic of metastatic papillary thyroid carcinoma. J Clin Ultrasound 2003;31:21–25.
115. Harrison LB, Zelefsky MJ, Pfister DG, et al. Detailed quality of life assessment in patients treated with primary radiotherapy for squamous cell cancer of the base of the tongue. Head Neck 1997;19:169–175.
116. Lin A, Kim HM, Terrell JE, Dawson LA, Ship JA, Eisbruch A. Quality of life after parotid-sparing IMRT for head-and-neck cancer: a prospective longitudinal study. Int J Radiat Oncol Biol Phys 2003;57:61–70.
117. Buus S, Grau C, Munk OL, Bender D, Jensen K, Keiding S. 11C-methionine PET, a novel method for measuring regional salivary gland function after radiotherapy of head and neck cancer. Radiother Oncol 2004;73:289–296.
118. Howlett DC, Alyas F, Wong KT, et al. Sonographic assessment of the submandibular space. Clin Radiol 2004;59:1070–1078.
119. Nomayr A, Lell M, Sweeney R, Bautz W, Lukas P. MRI appearance of radiation-induced changes of normal cervical tissues. Eur Radiol 2001;11:1807–1817.
120. Capaccio P, Paglia M, Minorati D, Manzo R, Ottaviani F. Diagnosis and therapeutic management of iatrogenic parotid sialocele. Ann Otol Rhinol Laryngol 2004;113:562–564.
121. Gritzmann N. Sonography of the salivary glands. AJR Am J Roentgenol 1989;153:161–166.

US of the Major Salivary Glands: Anatomy and Spatial Relationships, Pathologic Conditions, and Pitfalls

Ewa J. Bialek, MD, PhD, et al

RadioGraphics 2006; 26:745–763 • **Published online** 10.1148/rg.263055024 • **Content Codes:** HN NR US

Page 751
In acute inflammation, salivary glands are enlarged and hypoechoic. They may be inhomogeneous; may contain multiple small, oval, hypoechoic areas; and may have increased blood flow at US (Figs 12, 13) (9,22–25).

Page 751
In chronic inflammation, salivary glands are normal sized or smaller, hypoechoic, and inhomogeneous and usually do not have increased blood flow at US (Fig 14) (9,22,24).

Page 753
US features of sialolithiasis include strongly hyperechoic lines or points with distal acoustic shadowing, which represent stones (Fig 15) (22). In symptomatic cases with duct occlusion, dilated excretory ducts are visible (22).

Page 754
The most common benign neoplasms of major salivary glands are pleomorphic adenomas (mixed tumor) and Warthin tumors (adenolymphoma, cystadenolymphoma, papillary cystadenoma lymphomatosum). When their US appearance is analyzed, many common features may be found, but definitive differential diagnosis is usually not possible with US even between benign and malignant tumors.

Page 755
US features of a cyst are classic (like in any other location in the body): well-defined margins, anechoic content, posterior acoustic enhancement, and no evidence of internal blood flow at power Doppler or color Doppler imaging (Fig 33) (22).